

2 **BOND PERFORMANCE OF NEAR SURFACE MOUNTED FRP BARS**

3 Shehab M. Soliman¹, Ehab El-Salakawy², and Brahim Benmokrane³

4

5 **ABSTRACT:** Near surface mounted (NSM) reinforcement becomes now a well-known
6 method for strengthening existing concrete structures. The bond between the NSM
7 reinforcing bars and concrete is the key factor in the NSM technique. In the NSM
8 technique, there are two bond interfaces; one between the NSM bar and the adhesive, and
9 the other between the adhesive and the concrete. For this technique to perform efficiently,
10 these two interfaces need to be investigated. On the other hand, concrete structures that
11 require rehabilitation are often exposed to aggressive environments. Many of these
12 environments are related to cold-climate conditions as can be found in Canada.
13 Environmental factors including freeze/thaw action, exposure to de-icing salts, and
14 sustained low temperatures, combine to attack the integrity of repaired structures.
15 Consequently, repair materials for the Canadian infrastructure must be able to withstand
16 these harsh conditions for prolonged periods of time. A total of 80 NSM-FRP bars
17 installed in C-shaped concrete specimens were tested in pull-out setup to failure. Sixty
18 specimens were tested at normal room temperature, while the remaining 20 specimens
19 were tested after conditioning in an environmentally-controlled chamber for 200
20 freeze/thaw cycles. The dimensions of the specimens were designed, upon a preliminary
21 phase of testing, to ensure that no transverse cracking would occur in the specimen before
22 bond failure of the NSM bar. The results are presented in term of failure load, average
23 bond stress, strains in FRP bar, end slip, and mode of failure. A bond-slip model was
24 proposed for the used FRP bars.

1 **CE Database Subject Headings:** Fibre reinforced polymer (FRP); Near Surface
2 mounted (NSM); Pullout test; Freeze/thaw cycles; Bond slip model.

3 ¹ Ph. D. Candidate, Department of Civil Engineering, University of Sherbrooke, Sherbrooke,
4 Quebec, Canada J1K 2R1, Phone: (819) 821-8000 ext. 65178, Fax: (819) 821-7974, E-mail:
5 Shehab.Soliman@USherbrooke.ca

6 ² Associate Professor and Canada Research Chair in Advanced Composite Materials and Monitoring
7 of Civil Infrastructures, Department of Civil Engineering, University of Manitoba, Winnipeg,
8 Manitoba, Canada, R3T 5V6, Tel: (204) 474-8319 Fax: (204) 474-7513 E-mail:
9 Ehab_Elsalakawy@Umanitoba.ca

10 ³ NSERC Research Chair Professor in Innovative FRP Composite Materials for Infrastructures,
11 Department of Civil Engineering, University of Sherbrooke, Sherbrooke, Quebec, Canada, J1K 2R1,
12 Phone: (819) 821-7758, Fax: (819) 821-7974, E-mail: Brahim.Benmokrane@USherbrooke.ca

13

1 INTRODUCTION

2 As we move into the twenty-first century, the renewal and upgrade of our concrete
3 infrastructure become topics of critical importance. Existing infrastructure may have to
4 carry larger loads, require change in use, or overcome errors made during the design or
5 construction phases. To maintain and rehabilitate the existing infrastructure, new and
6 cost-effective materials and techniques are required to successfully extend the useful
7 lives of structures (Green et al. 2003). Due to many advantages, one of the most common
8 ways to strengthen structures is to externally-bond (EB) Fibre-Reinforced Polymer (FRP)
9 sheets or laminates on the surface of the structure. However, a disadvantage of such a
10 technique is that the surface-bonded materials can be subjected to fire, accidents or
11 vandalism. If the FRP composite material is placed in slots in the concrete cover some of
12 these disadvantages can be overcome. This method is designated as Near Surface
13 Mounted (NSM) Reinforcement.

14 Experimental results indicate that the use of NSM-FRP reinforcement is one of the
15 promising strengthening techniques for concrete structures (De Lorenzis and Nanni 2002;
16 Hassan and Rizkalla 2003; Soliman et al. 2008). However, to reach a comfortable level of
17 acceptance, knowledge on long-term behaviour of NSM-FRP under various
18 environmental conditions is required. Since both techniques, EB and NSM, are heavily
19 dependent on bond characteristics between FRP materials and concrete, investigations on
20 bond performance are crucial. Furthermore, wet concrete exposed to cycles of freezing
21 and thawing is one of the major causes of loss of bond and consequently early loss of
22 strength.

1 Very few investigations were carried out to study the durability of the NSM-FRP
2 technique (La Tegola and Micelli 2003; Täljsten and Carolin 2007). La Tegola and
3 Micelli (2003) tested six beams strengthened with NSM-CFRP and GFRP bars using
4 epoxy adhesive. In these beams, the groove was formed during casting, which may have
5 affected the bond characteristics between the concrete and the adhesive. The beams were
6 exposed to freeze/thaw cycles, high temperature, and high relative humidity with indirect
7 UV exposure. Test results showed a reduction in the ultimate deflection for the
8 conditioned beams. No effect was observed in either the serviceability performance or the
9 ultimate load carrying capacity of the beams. Täljsten and Carolin (2007) tested eight
10 beams in sub zero temperatures. Test results showed that the strengthened beams loaded
11 in cold climates can carry higher loads.

12

13 **BACKGROUND**

14 During the last few years, an extensive research work to investigate, develop and
15 implement sand-coated FRP bars, locally manufactured in Canada (Pultrall Inc. 2006), in
16 new concrete structures has been going at the University of Sherbrooke (El-Ragaby et al.
17 2007; El-Salakawy et al. 2003, Benmokrane et al. 2006 and 2007). However, the use of
18 these FRP bars in strengthening of existing structures is still to be investigated.
19 Therefore, the main objectives of this research project are: (1) to develop/utilize a NSM
20 system composed of the recently developed FRP bars and adhesives manufactured and
21 produced in Canada (Hilti Inc. 2006); (2) to investigate the effect of different parameters
22 on the bond performance of the proposed NSM system; and (3) to investigate the effect
23 of freeze/thaw cycles on the bond performance of the proposed NSM system. The above

1 objectives have been achieved through a series of pull-out tests carried out on concrete
2 specimens with NSM-FRP bars.

3

4 **EXPERIMENTAL PROGRAM**

5 **Material Properties**

6 All tested specimens were constructed using a ready-mixed concrete with a targeted 28-
7 day concrete compressive strength of 35 MPa. The actual concrete compressive and
8 tensile strengths were determined based on standard cylinder tests (150×300 mm), at the
9 same time of testing the specimens. The obtained concrete compressive strength ranged
10 between 38 and 44 MPa with a standard deviation of 2.85 MPa. The average concrete
11 tensile strength ranged between 2.9 and 3.6 MPa with a standard deviation of 0.29 MPa.

12 Two types of sand-coated FRP bars, carbon and glass, were used in this study (Pultrall
13 Inc. 2006). Two sizes, No.10 (9.5-mm diameter) and No.13 (12.7-mm diameter), were
14 used for carbon, while only size No.13 (12.7-mm diameter) was used for glass. All FRP
15 bars were tested to obtain the tensile strength and modulus of elasticity according to ACI
16 440.3R-04 guidelines (ACI Committee 440 2004). The obtained tensile properties for the
17 used FRP bars are presented in Table 1. The average longitudinal tensile strength, f_{fu} ,
18 was 1546 ± 112 , 1250 ± 57 and 749 ± 27 with a corresponding modulus of elasticity equals
19 128 ± 11.2 , 134 ± 12.1 and 42 ± 1 GPa for CFRP No.10, No.13 and GFRP No.13,
20 respectively.

21 Two adhesive types were used in this study (Hilti Inc. 2006). The first type, HIT RE 500,
22 is a high strength epoxy based adhesive consisting of two parts; resin and hardener. This
23 type is specially designed for fastening into solid base materials in a wide range of

1 material temperatures ranging from 49°C down to -5°C. It may be also used in
2 underwater fastening for oversized holes up to twice the bar diameter but with a
3 maximum hole diameter of 76 mm. The HIT RE 500 can be used on wet or dry surfaces
4 and is characterized by having excellent weathering resistance and high temperature
5 resistance. The second type of adhesive, HIT HY 150, is a hybrid adhesive consisting of
6 methacrylate resin, hardener, cement and water. It is formulated for fast curing and
7 installation in a wide range of material temperatures ranging from 40°C down to -5°C.
8 The manufacturers' specifications of the used adhesives are listed in Table 2.

9

10 **Test Specimens**

11 A total of 80 C-shaped concrete specimens were constructed and tested in the laboratory.
12 The configuration of the specimens used in this study is similar to that developed by
13 De Lorenzis et al. (2002). The typical specimen consisted of a C-shaped concrete block
14 with outside dimensions of 340 × 340 mm, inside dimensions of 170 × 170 mm, and a
15 height of 500 mm. Following the 28-day curing period, the groove was formed by
16 making two saw cuts and removing the concrete in between by a light-weight power
17 hammer. On the other hand, each FRP bar was cut to the required length and a steel
18 anchor was installed at one end of the bar. The anchor consisted of a 25.4-mm diameter
19 steel sleeve with a length of $40d$ (d is the nominal diameter of the FRP bar) filled with
20 high performance resin grout.

21 Before the installation of the FRP bars, pressurized air was used to ensure that the groove
22 is clean. The adhesive was injected into the groove covering $2/3$ of its depth. The bar was
23 gently inserted into the groove over foam supports outside the bonded length to maintain

1 the thickness of the adhesive and then gently pressed to displace the bonding agent. Extra
2 adhesive was added to fill the groove as needed. The excess adhesive was then removed.
3 Different parameters were investigated in this study including: the bonded length ($6d$,
4 $12d$, $18d$, $24d$, $36d$ and $48d$); type of FRP bars (carbon and glass); size of FRP bars
5 (No.10 and No.13); groove width ($1.5d$ and $2.0d$); type of adhesive (epoxy and cement-
6 based); environmental conditions (normal room temperature and 200 freeze/thaw cycles).
7 Each specimen was given a designation in the format X/Y-00-Z-0.0-00. The first
8 character X represents the condition of the specimens whether it is tested in normal room
9 temperature, N, or tested after being subjected to freeze/thaw cycles, F. The second
10 character, Y, represents the type of FRP bar, C for carbon and G for Glass. The first 2-
11 digit number represented the bar size; 10 and 13, respectively. The third character, Z,
12 represents the type of adhesive, E for epoxy and C for cement. The second number
13 represents the groove depth as a multiple of the bar diameter whether 1.5 or 2.0. The third
14 number represents the bonded length also as a multiple of the bar diameter whether 6, 12,
15 18, 24, 36 or 48.

16 The testing was carried out on two phases. The first phase included testing of 60
17 specimens at normal room temperature. In this phase, three replicate specimens were
18 tested for each test parameter, however only the average values obtained from the three
19 replicates are reported. The second phase included testing of 20 conditioned specimens,
20 with two replicates, where they were subjected to 200 freeze/thaw cycles in a controlled
21 environmental chamber before testing. Tables 3 and 4 summarize the test parameters.

22

23

1 **Test Setup and Instrumentation**

2 The FRP-NSM, C-shaped concrete specimens were tested in a pullout setup using a
3 BALDWIN hydraulic machine as shown in Fig. 1. The applied load was reacted by
4 means of four steel threaded bars inserted into holes (30-mm in diameter) near the
5 corners of the specimen. The concrete specimens were encapsulated in between two steel
6 plates to avoid any concentration of stresses at the threaded bar location during testing.

7 Each specimen was instrumented with two high accuracy (± 0.001 mm) linear variable
8 displacement transducers (LVDTs) to measure the free and the loaded end slips of the
9 FRP bar. Three electrical-resistance strain gauges (EG) with gauge length of 6.0 mm
10 were attached to the bar to capture the strain distribution along the bonded length. To
11 avoid affecting the bonded length, the EG were installed on the outer surface of the FRP
12 bars. Reading from the machine load cell, LVDTs and EGs were collected using an
13 automatic data acquisition system connected to a computer.

14

15 **Freezing and thawing cycles**

16 Before conditioning the specimens in the environmental chamber, service cracks were
17 developed in each of the 20 specimens. The specimens were tensioned to 30% of the
18 failure load, which represents the allowable service load level according to the
19 CAN/CSA-S6-06 code (CSA 2006). Afterwards, 200 freeze/thaw cycles were performed
20 in the walk-in controlled environmental chamber (3.70×2.60 m). During the freezing
21 process, the lower bound was set to -20°C for 12 hours at 80% relative humidity. While
22 during the thaw process, the temperature was raised to $+25^{\circ}\text{C}$ for 6 hours at 100%
23 relative humidity.

1 In addition to EGs, thermocouples were placed in two positions in the specimens; at the
2 bar-epoxy interface and in the epoxy-concrete interface to capture the temperature at
3 these interfaces. All the wires of the strain gauges and the thermocouples were collected
4 outside the environmental chamber and connected to a data acquisition system (DAQ).
5 For the first 20 cycles, Readings were acquired every minute to capture the change in
6 strain due to change in the temperature. Afterwards, due to lack of DAQ, readings from
7 the strains were taken manually by using a strain indicator box (P-3500) till the end of the
8 200 cycles. Table 4 summarizes the test parameters for the freeze- thaw investigation.

9

10 **TEST RESULTS AND DISCUSSION**

11 The test results of these specimens were presented in terms of failure load, mode of
12 failure and average bond stress as summarized in Tables 3 and 4.

13

14 **Failure Load**

15 Figure 2 shows comparison between the failure load of the conditioned and reference
16 specimens. For specimens with epoxy adhesive, the failure load for most of the
17 conditioned specimens was slightly reduced. The percentage of reduction for those
18 specimens varied between 8 and 14 %. Only two specimens gained an increase in the
19 failure load, F/C-10-E-1.5-12 and F/C-10-E-2.0-18. This increase was about 4.6% and
20 7.5%, respectively. It is noted from Fig. 4 that the percentage of reduction for specimens
21 with a groove width equals to $1.5d$ was greater than specimens with groove width equals
22 to $2.0d$. Since failure was due to splitting of epoxy, increasing the groove width from
23 $1.5d$ to $2.0d$, enhances the resistance to splitting.

1 As shown in Fig. 3 , the ultimate loads for reference specimens with cement adhesive
2 were 40 to 56% less than their counterparts with epoxy adhesive. However, the failure
3 loads for the conditioned specimens with cement adhesive was about 30 to 45% less than
4 those of reference (unconditioned) specimens.

5 Furthermore, for a given groove size, as the bonded length was increased the ultimate
6 load required to pullout the bar was increased as shown in Fig. 4. As well, the average
7 bond stress was decreased due to the non-uniform distribution of the bond stresses on the
8 longer bonded length.

9 For specimens tested in normal room temperature with epoxy adhesive, increasing the
10 groove size from $1.5d$ to $2.0d$ had insignificant effect on the pullout load at failure as
11 shown in Fig. 4. This was due to the fact that failure was mostly controlled by the tensile
12 strength of concrete not the splitting of the epoxy cover. Even when it occurred in some
13 specimens, it was following the formation of the inclined cracks in concrete.

14

15 **Modes of Failure**

16 **Specimens with epoxy adhesive**

17 The common mode of failure for most of the specimens using epoxy as an adhesive
18 material was concrete shear-tension failure (semi-cone failure) as shown in Fig. 5a. The
19 failure was either accompanied with or without cracking in the epoxy, depending on the
20 bonded length. This shear-tension failure mode was due to tensile stresses along the
21 inclined planes in the concrete surrounding the groove. Internal longitudinal cracks were
22 observed in the epoxy in many specimens at failure. These cracks indicated the path of
23 the tension force in the bar. This tensile force was transferred to the epoxy. As a result of

1 the fact that the tensile strength of the epoxy was much higher than that of concrete, most
2 of the failure was in the concrete. These cracks started at the loaded end and then
3 propagated to the free end. Once a crack reached the free end, the epoxy cover suddenly
4 split Fig. 5b).

5 Furthermore, at the same loading level, as the bonded length increases the tensile stresses
6 in the epoxy adhesive decrease. If the bonded length is long enough to develop the full
7 strength of the FRP bar, bar rupture occurs before the epoxy reaches its tensile strength.
8 Therefore, for specimens with bonded length longer than $18d$, namely N/C-10-E-1.5-24,
9 N/C-10-E-1.5-36, N/C-10-E-1.5-48 and N/G-13-E-2.0-36, FRP bar rupture was observed
10 as shown in Fig. 8a. While, specimens N/C-13-E-1.5-18 and N/C-13-E-2.0-18 failed by
11 bar slip due to bond failure at the epoxy/FRP bar interface as shown in Fig. 6b.

12 On the other hand, the modes of failure for specimens with a GFRP bars were similar to
13 their counterparts with a CFRP bars. Specimen N/G-13-E-2.0-12 with the smallest
14 bonded length failed by bar slip at the bar-epoxy interface (Fig. 6b). While, specimens
15 N/G-13-E-2.0-18 and N/G-13-E-2.0-24 failed by concrete rupture accompanied by
16 peeling off the epoxy layer with a portion of concrete surrounding the groove.

17 Opposite to reference specimens, different modes of failure were obtained for the
18 conditioned ones. The mode of failure of each conditioned specimen is given in Table 4.
19 The reference specimen N/C-10-E-1.5-12 failed by concrete tension failure (Fig. 5b),
20 while its conditioned counterpart failed by epoxy splitting (Fig. 7a) showing higher slip.
21 Figure 8 shows a comparison between the average bond stress-slip for conditioned, F/C-
22 10-E-1.5-18 and its reference specimen, N/C-10-E-1.5-18, which showed higher slip for
23 the conditioned one. For specimen F/C-10-E-1.5-18, two diagonal cracks were initially

1 formed between the corner of the specimen and the groove at approximately 45 degrees.
2 The width of these cracks enlarged and further propagated with increasing the load till it
3 reached the epoxy layer. When the tensile stress reached the tensile strength of the epoxy,
4 cracks started to appear in the epoxy till the specimen failed. This mode of failure was the
5 common mode of failure for most of the conditioned specimens with epoxy adhesive
6 (Fig. 7b).

7 The variation of the results between conditioned and unconditioned (reference)
8 specimens, either in failure load or in failure mode, was due to the difference in values of
9 thermal expansion coefficient between the adhesive material and the concrete.

10

11 **Specimens with cement adhesive**

12 The main mode of failure was adhesive splitting at the concrete-cement interface. The
13 failure occurred at low load levels compared to the epoxy adhesive as given in Table 3.

14 The failure load for the specimens with a groove size equal to $2.0d$ was lower than that of
15 the specimens with groove size of $1.5d$. This was due to the fact that shrinkage of the
16 cement in a bigger groove size was greater than that of the smaller groove size, which
17 accelerated the debonding of the cement from the concrete (Hilti Inc.2006). Furthermore,
18 the mode of failure for the conditioned specimens was the same as their counterpart
19 reference specimens. However, the failure load was lower compared to the reference
20 specimens.

21

22 **BOND-SLIP ANALYSIS**

23 **Average Bond Stress-Slip Relationship**

1 The bond stress is calculated by dividing the pullout force by the failure contact area.
2 Therefore, when the failure is at the FRP-adhesive interface for slip or splitting of the
3 adhesive layer, the average bond stress is calculated using the following equation (De
4 Lorenzis et al. 2002)

$$5 \quad \tau_{av} = \frac{P_u}{\pi \cdot d \cdot L_b} \quad (1)$$

6 However, if the failure is at concrete-adhesive interface, the average bond stress is
7 calculated by the following equation (De Lorenzis et al. 2002):

$$8 \quad \tau_{av} = \frac{P_u}{(d_g + 2h)L_b} \quad (2)$$

9 Where τ_{av} is the average bond stress, P_u , pullout load at failure, d is the diameter of FRP
10 bar, d_g is the width of the groove, h is the height of the groove and L_b is bonded length of
11 FRP bar in concrete.

12

13 The average bond stress-slip relationship can be divided into four stages (Fig. 8). In the
14 first stage, the average bond stress increases linearly up to 50 to 60% of the ultimate bond
15 stress. In this first stage, no cracks were observed neither in the epoxy nor in the concrete
16 since the bar and the adhesive material were in the elastic state. In the second stage,
17 starting just above 50-60% of the ultimate bond stress, a crackling noise was recognized,
18 which represents the starting of microcracks in the epoxy and concrete surrounding the
19 groove. As the load increased, these cracks increased (became visible) and relative slip
20 between the adhesive-FRP bar and/or adhesive-concrete interfaces occurred. This stage
21 represents the nonlinear part of the curve up to the ultimate bond stress. In the third stage,
22 beyond the ultimate bond stress, a yielding plateau occurred with a large slip followed by

1 linear decrease in the last stage. The difference in slip value shown in bond stress-slip
2 diagrams between the loaded-end slip and the free-end slip at the ultimate bond stress
3 was due to the elastic elongation of the FRP bar.

4

5 **Local Bond Stress-Slip Relationship**

6 It is important to evaluate the local bond slip as it defines the relationship between the
7 applied stress and the corresponding slip value. According to the literature, there are
8 many ways that can be used to measure the local bond stress-slip relationship (Focacci et
9 al. 2002; Teng et al. 2006). Depending on the available experimental data, the local bond
10 stress-slip can be identified by:

- 11 - the average bond stress-slip for small bonded length;
- 12 - reading from strain gauges placed along the FRP rod;
- 13 - by using numerical identification.

14 In this investigation, the readings from the strain gauges are used to obtain the local
15 bond-slip relationship, which in turn can represent the behaviour of the bond between the
16 FRP bar and the adhesive.

17 The force, P_u , acting on a piece of FRP bar of length dx is shown in Fig. 9. It is assumed
18 that the behaviour is linearly elastic, therefore, the bond stress, τ , applied on the FRP bar
19 can be calculated using equation (1) above, with $L_b = dx$.

$$20 \quad \tau = \frac{P_u}{\pi d dx} \quad (3)$$

$$21 \quad E_f = \frac{\frac{P_u}{\pi d^2} / 4}{d \varepsilon_f(x)} \quad (4)$$

1
$$\tau = \frac{d}{4} \cdot E_f \cdot \frac{d\varepsilon_f(x)}{dx} \quad (5)$$

2
$$\tau_{\left(\frac{x_i+x_j}{2}\right)} = \frac{d}{4} \cdot E_f \cdot \frac{\varepsilon_{fj} - \varepsilon_{fi}}{x_{fj} - x_{fi}} \quad (6)$$

3 Where x is the coordinate along the longitudinal axis of the FRP bar within the bonded
 4 length, E_f , d and ε_f are the Young's modulus, bar diameter and strain in the FRP bar,
 5 respectively. Therefore, the bond stress profile diagram at a given load level can be
 6 obtained from the first derivative of the strain profile at that load level multiplied by E_f
 7 and d .

8 Figures 10 and 11 show the strain distribution along the bar bonded length for specimens
 9 N/C-10-E-1.5-48 and N/G-13-E-2.0-36, respectively. Each curve is corresponding to a
 10 specific load represented as a percentage of the ultimate load. The x-axis started from the
 11 free-end to the loaded-end along the bonded length of the bar. The strain distribution
 12 along the bond length, highly nonlinear at lower load levels, gradually approached an
 13 almost linear shape as the load increased. This means that, as the load increased,
 14 redistributions of the bond stress along the bond length occurred as a result of the
 15 changes in the state of the bond. Microcracking at the bar–adhesive interface and the
 16 consequent slip of the FRP tend to produce a more even distribution of the bond stress.

17

18 Therefore, applying equations 6 on Fig. 10 and 11 at each load level, the local bond stress
 19 can be obtained. Figures 12 and 13 show the bond stress distribution along the bar
 20 bonded length for specimens N/C-10-E-1.5-48 and N/G-13-E-2.0-36 corresponding to a
 21 specific load represented as a percentage of the ultimate load. At low load levels, the
 22 bond stress at the bar free-end was close to zero. As the load increases, the peak of the

1 bond stress gradually shifts towards the free-end. The presence of more than one peak in
 2 the bond stress distributions during the last loading stages is probably related to the
 3 presence of transverse concrete cracks, which introduce local disturbances to the bond
 4 behaviour. As can be seen from the two figures, the bond stress for the specimens with
 5 CFRP bars are much higher than those for specimens with GFRP due to the difference in
 6 axial stiffness (EA) between carbon and glass bars.

7

8 Now, from the definition of slip:

$$9 \quad S_l = u_f - u_e - u_c \quad (7)$$

10 Where u_f , u_e and u_c are the displacements of FRP bar, adhesive and concrete,
 11 respectively. Since,

$$12 \quad \varepsilon_f = \frac{du_f}{dx}, \varepsilon_e = \frac{du_e}{dx} \text{ and } \varepsilon_c = \frac{du_c}{dx} \quad (8)$$

13 and by assuming that the adhesive strain, ε_e and concrete strain, ε_c are very small and
 14 may be considered negligible when compared to that of the FRP, ε_f , which can be
 15 calculated as follows:

$$16 \quad \varepsilon_f = \frac{dS_l}{dx} \quad (9)$$

$$17 \quad S_l(x) = S_l(0) + \int_0^x \varepsilon_f(x) dx \quad (10)$$

$$18 \quad S_l(x_i) = S_l(0) + \sum_{x=0}^{x=l_b} \varepsilon_f(x) \quad (11)$$

1 where $S_f(0)$ is the free-end slip of the FRP bar. Therefore, the slip profile for each given
2 load level can be obtained by integrating the strain versus location curve and adding the
3 free-end slip at that load level. Thus applying equation 11 on Figures 10 and 11 at each
4 load level, the local slip can be obtained.

5

6 Therefore, using the previous analogy, the local bond-slip curves can be drawn. Figures
7 14 and 15 show the local bond stress-slip relationship, at the location of each strain
8 gauge, for specimens N/C-10-E-1.5-48 and N/G-13-E-2.0-36, respectively.

9

10 **NONLINEAR REGRESSION ANALYSIS**

11 In this section, statistically based analysis is presented to predict the failure load for the
12 pullout specimens with NSM-FRP bar. A simple regression model or a mathematical
13 equation can be used to set up a simplified model that best fits the experimental data in
14 terms of failure load. One of the tools that can be used in developing such a model is the
15 response surface methodology (RSM) and nonlinear statistical regression analysis. An
16 application of this methodology on two way slabs has been presented by Ebead et al.
17 (2002). A RSM is built up by simulating solutions at systematic points in a design space
18 of various parameters and setting up a model to these points. We aim to use such models
19 as design equations similar to those in the currently available specifications and
20 guidelines.

21 The DataFit software, Version 8.1.69 is used for the calculations associated with the
22 nonlinear regression analysis (DataFit 2005). Generally, the goal of the nonlinear
23 regression analysis is to determine the best-fit parameters for a model by minimizing the

1 chosen test function. This function defines the difference between the actual and
2 predicted responses and is given by:

$$3 \quad x^2 = \sum_{i=1}^{i=N} [y_i - y(F_i)]^2 \quad (12)$$

4 Where N is the total number of random input data, y_i is the actual response value (output
5 of a particular RSM model) and $y(F_i)$ is the response value computed from the proposed
6 nonlinear regression model.

7 Nonlinear regression analysis is essential when the response model exhibits a nonlinear
8 dependence on the unknown variables (five variables in this study). Hence, the process of
9 test function minimization is an iterative process. This iterative process begins with some
10 initial estimates and incorporates algorithms to improve the estimates in an iterative
11 manner. The new estimates then became a starting point for the next iteration. These
12 iterations continued until the values of the test function converge (Datafit 2005). Below,
13 the nonlinear regression model (referred to as the proposed design equations) is
14 presented.

15 In the following sections, the five variables used to perform the statistical analyses are
16 elaborated upon. Then the RSM models for the five different responses are presented and
17 considered in the RSM models. The design equation for the pullout load is predicted in
18 term of axial stiffness of FRP bar, tensile strength and modulus of elasticity of adhesive,
19 groove width and bonded length.

$$20 \quad P_u = -1.25(EA)_{frp} + 1.7 f_{ta} + 0.0028E_a - 1.52dg + 0.137 * Lb \quad (13)$$

21 Where, P_u , is the pullout load at failure in kN, EA is the axial stiffness of the FRP bar in
22 MN, f_{ta} is the tensile strength of the adhesive in MPa, E_a is the modulus of elasticity of

1 adhesive in GPa, d_g is the width of the groove in mm, and L_b is the bond length of FRP
2 bar in mm.

3 Using the proposed model, Fig. 16 shows a comparison between the experimentally
4 measured and the predicted failure load. In this figure, the coefficient of determination,
5 R^2 , equals 0.85, which indicates good prediction capability of the proposed equation.
6 Accordingly, this equation can be employed to predict the capacity of pullout test
7 specimens or in other applications where the force transfers from the FRP to the concrete
8 element through direct shear.

9

10 **CONCLUSIONS**

11 The experimental program has provided an understanding of the bond behaviour of the
12 NSM-FRP bar technique in concrete elements and the effect of one of the most severe
13 environmental conditions; the freeze/thaw cycles, on that behaviour. Based on the
14 experimental results, the following conclusions can be drawn:

- 15 • The adopted system, FRP V-ROD™ bars and Hilti adhesives, seems to perform well
16 in the NSM strengthening system.
- 17 • The adopted test methods seem to be efficient and produced consistent results.
- 18 • The main mode of failure for most of the tested specimens with epoxy adhesive was
19 concrete tension failure (semi-cone failure) accompanied with or without epoxy
20 cracking (splitting). Specimens with longer bonded length failed by bar rapture.
- 21 • The main mode of failure for the specimens with cement adhesive was adhesive
22 splitting at the concrete-cement interface. These specimens showed a failure load of
23 about 40 to 56% of that of their counterparts with epoxy adhesive.

- 1 • Increasing the bonded length increased the pullout/failure load and the bond stress
2 was decreased due to longer length distribution.
- 3 • Increasing the groove size for specimens with epoxy adhesive did not have a
4 significant influence on the failure load. However, the factor that controlled failure
5 was the tensile strength of concrete.
- 6 • Increasing the groove size for specimens with cement adhesive decreased the failure
7 load; this was due to greater shrinkage of cement in bigger groove size. Therefore, it
8 is not recommended to use groove size greater than 1.5 times the bar diameter when
9 cement adhesive is used.
- 10 • Due to temperature change during freeze/thaw cycling, hair cracks developed in the
11 adhesive materials. Therefore, the properties of the adhesive material are expected to
12 govern the mode of failure of the specimens as well as the slip performance. For the
13 conditioned specimens with epoxy adhesive, the failure load was reduced by 8 to 14
14 % compared to the counterpart reference specimens. While, for the conditioned
15 specimens with cement adhesive, this reduction was about 30 to 45%.
- 16 • The change of strain due to freeze/thaw cycling was around 70 to 90 micro-strain in
17 case of epoxy adhesive and around 120 to 170 micro-strains in case of cement
18 adhesive.
- 19 • During freeze/thaw cycles, the measured change in strain increased with the increase
20 in bonded length. While, changing the groove width had no effect on the change of
21 strain with temperature.
- 22

1 **ACKNOWLEDGEMENT**

2 The authors would like to express their special thanks and gratitude to the Natural
3 Science and Engineering Research Council of Canada (NSERC), ISIS Canada, Pultrall
4 Inc. (Thetford Mines, Québec), Hilti Inc. (Montréal, Québec), and the technical staff of
5 the structural lab in the Department of Civil Engineering at the University of Sherbrooke.

6

7 **REFERENCES**

- 8 ACI Committee 440. (2004). “Guide Test Methods for Fiber-Reinforced Polymers
9 (FRPs) for Reinforcing or Strengthening Concrete Structures”, ACI 440.3R-04, American
10 Concrete Institute, Farmington Hills Michigan, 40 p.
- 11 Asplund, S. (1949). “Strengthening Bridge Slabs with Grouted Reinforcement”, *ACI*
12 *Structural Journal*, American Concrete Institute, 20(6), 397-406.
- 13 Benmokrane, B., El-Salakawy, E.F., El-Ragaby, A. and Lackey, T. (2006). “Designing
14 and testing of concrete bridge decks reinforced with glass FRP bars.” *ASCE, Journal of*
15 *Bridge Engineering*, 11(2), 217–229.
- 16 Benmokrane, B., El-Salakawy, E.F., El-Gamal, S.E., and Sylvain, G. (2007).
17 “Construction and Testing of an Innovative Concrete Bridge Deck Totally Reinforced
18 with Glass FRP Bars: Val-Alain Bridge on Highway 20 East.” *ASCE Journal of Bridge*
19 *Engineering*, 12(5), 632-645.
- 20 Canadian Standard Association (CSA), (2006). ”Canadian High-Way Bridges Design
21 Code.” *CAN/CSA-S6-06, Canadian Standard Association*, Rexdale, Ontario, Canada.
- 22 Cruz JM S., Barros JAO. (2006). “Bond between Near Surface Mounted Carbon Fiber

1 Reinforced Polymer Laminate strips and Concrete”, ASCE, *Journal of Composites for*
2 *Construction*, 8(6), 519-527

3 DataFit. (2005). “Datafit Curve Fitting (Nonlinear Regression) and Data Plotting
4 Software.” *version 8.1.69*. Oakdale Engineering, Inc, Oakdale, PA, USA, 2005.

5 De Lorenzis, L., Nanni A. (2002). “Bond between NSM Fiber-Reinforced Polymer Rods
6 and Concrete in Structural Strengthening”, *ACI Structural Journal*, 99(2), 123–132.

7 De Lorenzis, L., Rizzo, A., and La Tegola, A. (2002). “A modified pull-out test for bond
8 of near-surface mounted FRP rods in concrete.” *Composites Engineering Part B.*, 33, (8),
9 589-604.

10 Design-Expert. (2000). “Design of Experiments (DOE) Software.” *version 6.0.1*. Stat-
11 Ease, Inc, Minneapolis, MN, USA, 2000.

12 El-Hacha, R., Rizkalla, S. (2004). “Near Surface Mounted Fiber Reinforced Polymer
13 Reinforcements for Flexural Strengthening of Concrete Structures”, *ACI Structural*
14 *Journal*, American Concrete Institute, 101(5), 717-716.

15 El-Ragaby, A., El-Salakawy, E.F., and Benmokrane, B. (2007). “Fatigue Performance of
16 FRP Reinforced Concrete Bridge Deck Slabs.” *ASCE Journal of Composites for*
17 *Construction*, 11(3), 258-268.

18 El-Salakawy, E.F., Benmokrane, B., and Desgagné, G. (2003). “FRP Composite Bars for
19 the Concrete Deck Slab of Wotton Bridge.” *Canadian Journal of Civil Engineering*,
20 30(5), 861-870.

21 Focacci, F., Nanni, A. and Bakis, C., Local Bond-Slip Relationship For FRP
22 Reinforcement in Concrete.” *ASCE Journal of Composites for Construction*, 4(1), 24-31.

1 Green, M., Bisby, L., Beaudoin, Y., and Labossiere, P. (2003). "Effect of Freeze-Thaw
2 Cycles on the Bond Durability between Fibre Reinforced Polymer Plate Reinforcement
3 and Concrete." *Canadian Journal of Civil Engineering*, 27, (5), 949-959.

4 Hassan T., Rizkalla S. (2003). "Investigation of Bond in Concrete Structures
5 Strengthened with Near Surface Mounted Carbon Fibber Reinforced Polymer Strips",
6 *Journal of Composites for Construction*, ASCE, 7(3), 248–257.

7 Hilti Inc. (2006). Product Technical Guide, <http://www.ca.hilti.com>.

8 La Tegola, A. and Micelli, F. (2003). "Environmental Effect on RC Beams with Near
9 Surface Mounted FRP Rods." *Sixth International Symposium on FRP Reinforcement for*
10 *Concrete Structures (FRPRCS-6)*, 8-10 July, Singapore, 10 p.

11 Lundqvist, J. (2007). "Numerical Analysis of Concrete Elements Strengthened with
12 Carbon Fiber Reinforced Polymers" Doctoral Thesis, *Luleå University of Technology*,
13 Sweden, 138 p.

14 Pultrall Inc. (2006). "Product Technical Specifications", <http://www.Pultrall.com>.

15 Soliman, S.M., El-Salakawy E.F., and Benmokrane B. (2007). "Bond Properties of Near
16 Surface Mounted (NSM) Carbon FRP Bars in Concrete", *Annual General Meeting &*
17 *Conference Canadian Society of Civil Engineering*, June 6-9, Yellowknife, Northwest
18 Territories, Canada, 10p.

19 Soliman, S.M., El-Salakawy, E.F., and Benmokrane, B. (2008a). "Flexural Behaviour of
20 Concrete Beams Strengthened with Near Surface Mounted FRP Bars." *Fourth*
21 *International Conference on FRP Composites in Civil Engineering (CICE2008)*, 22-24
22 July, Zurich, Switzerland, 8 p.

- 1 Soliman, S.M., El-Salakawy E.F., and Benmokrane B. (2008b). “Effectiveness of Using
2 NSM CFRP Bars in Flexural Strengthening of Reinforced Concrete Beams”, *Annual*
3 *General Meeting & Conference, CSCE*, June 10-13, Quebec city, Quebec, Canada, 9p.
- 4 Taljten, B. and Carolin, A. (2007). “CFRP Strengthening of Concrete Beams– Testing in
5 Sub-Zero Temperature.” *International Journal of Materials and Product Technology*
6 (IJMPT), 28, (1/2), 29-45.
- 7 Teng, J.G., De Lorenzis, L., Wang, B., Li, R., Wong, T.N., and Lam, L. (2006).
8 “Debonding Failures of RC Beams Strengthened with Near Surface Mounted CFRP
9 Strips.” *Journal of Composites for Construction*, 10, (2), 92-105.

10

11

1

2 Table 1 - Mechanical properties of the used NSM reinforcing bars

Bar type	Bar diameter mm	Bar area mm ²	Modulus of elasticity, GPa	Tensile strength, MPa	Ultimate strain %
CFRP	9.5	71	128±11.2	1546±112	1.21±0.19
	12.7	127	134±12.1	1250±57	0.94±0.09
GFRP	12.7	127	42±1	749±27	1.80±0.04

3

4

5 Table 2 - Material specifications of adhesives (Hilti 2006)

Adhesive	Compressive Strength, MPa	Tensile Strength, MPa	Modulus of Elasticity, MPa	CTE x10 ⁶ °C ⁻¹	T _g	Bond Strength, MPa
Epoxy, HIT RE 500	82.7	43.5	1493	42.5	89	12.4
Cement, HIT HY 150	71.8	15.9	7032	29.5	–	Not Specified

6

7

1

2 Table 3 - Test results for unconditioned specimens

Specimen code	Type and diameter of FRP	Groove filling	Groove width	Bonded length	Pullout Load at, kN	Average bond stress, MPa	Mode of Failure
N/C-10-E-1.5-6	CFRP 9.5 mm	Epoxy	1.5d	6d	28.68	16.02	C
N/C-10-E-1.5-12				12d	52.45	14.65	C
N/C-10-E-1.5-18				18d	74.85	13.93	C+Se
N/C-10-E-1.5-24				24d	84.77	—	R
N/C-10-E-2.0-6	CFRP 9.5 mm	Epoxy	2.0d	6d	35.56	19.87	C
N/C-10-E-2.0-12				12d	59.35	16.58	C+Se
N/C-10-E-2.0-18				18d	64.57	12.10	C+Se
N/C-10-E-2.0-24				24d	75.62	10.56	C
N/C-10-E-2.0-36				36d	96.291	—	R
N/C-10-E-2.0-48				48d	96.23	—	R
N/C-13-E-1.5-18	CFRP 12.7 mm	Epoxy	1.5d	18d	48.83	5.36	S
N/C-13-E-2.0-18				2.0d	18d	49.05	5.38
N/G-13-E-2.0-12	GFRP 12.7 mm	Epoxy	2.0d	12d	52.19	10.90	S
N/G-13-E-2.0-18				18d	66.93	9.32	S
N/G-13-E-2.0-24				24d	77.74	8.12	C+E+S
N/G-13-E-2.0-36				36d	79.80	—	R
N/C-10-C-1.5-12	CFRP 9.5 mm	Cement	1.5d	12d	31.73	4.81	Ic-c
N/C-10-C-1.5-18				18d	32.45	3.25	Ic-c
N/C-10-C-1.5-24				24d	44.68	3.38	Ic-c
N/C-10-C-2.0-24				2.0d	24d	35.24	2.45

3 C = Concrete tension failure, R = Rupture of bar, S = Slip of bar, Se = Splitting of epoxy,

4 Sc = Splitting of Cement, Ic-c = failure at concrete–cement interface and E = epoxy

5 cracking.

6

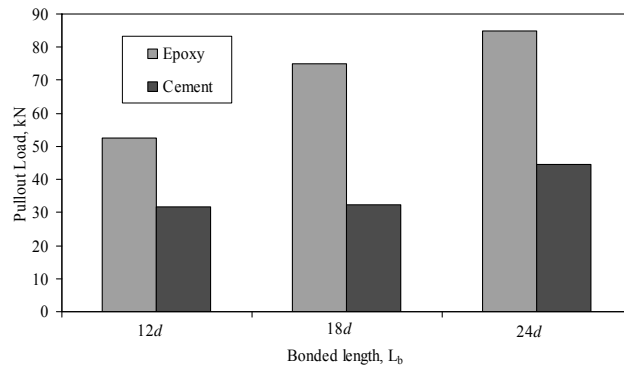
1 Table 4 - Test results for freeze/thaw conditioned specimens

Specimen code	Groove filling	Groove dimension	Bonded length	Pullout load, kN	Bond strength, MPa	Failure mode	% of change
F/C-10-E-1.5-12			12d	54.85	15.32	Se	4.58
F/C-10-E-1.5-18	Epoxy	1.5d	18d	63.82	11.89	C+Se	-14.74
F/C-10-E-1.5-24			24d	74.21	10.37	C+Se	-12.46
F/C-10-E-2.0-12			12d	52.24	14.59	Se	-11.98
F/C-10-E-2.0-18	Epoxy	2.0d	18d	69.39	12.92	Se	7.46
F/C-10-E-2.0-24			24d	69.53	9.71	C+Se	-8.05
F/C-10-C-1.5-12			12d	17.30	2.62	Ic-c	-45.48
F/C-10-C-1.5-18	Cement	1.5d	18d	17.56	1.77	Ic-c	-45.89
F/C-10-C-1.5-24			24d	31.35	2.38	Ic-c	-29.83
F/C-10-C-2.0-24			Cement	2.0d	24d	35.27	2.45

2 C = Concrete tension failure, Se = Splitting of epoxy cover and Ic-c = concrete-cement

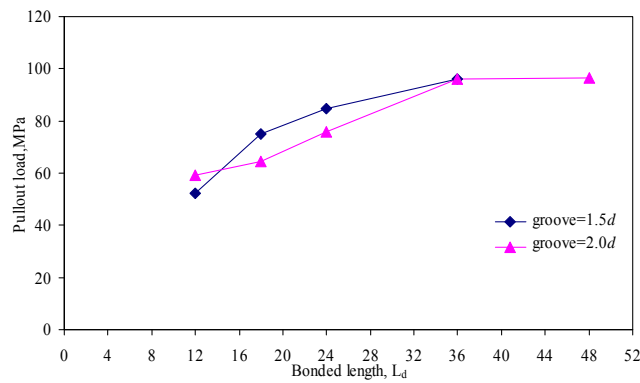
3 interface failure.

4



1
2

Fig. 3 - Pullout load for epoxy and cement adhesive for groove size of 1.5d



3
4

Fig. 4 - Pullout load at failure versus bonded length for epoxy adhesive



5
6
7
8

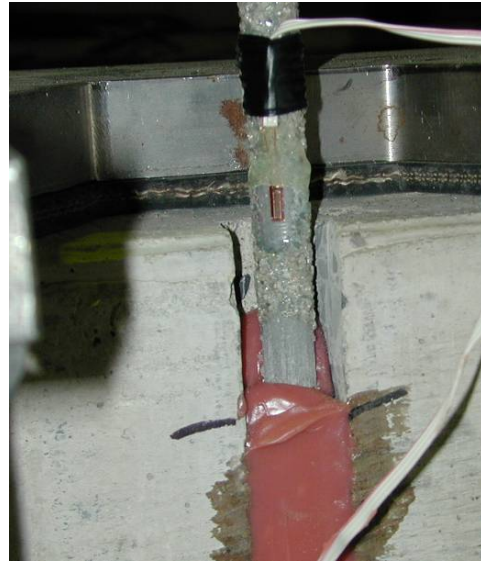
a) Concrete tension failure for N/C-10-E-1.5-12

b) Concrete tension failure with epoxy cracking for N/C-10-E-2.0-18

Fig. 5 - Mode of failure for specimens with NSM-CFRP bar and epoxy adhesive.



a) Bar rupture for N/G-13-E-2.0-36

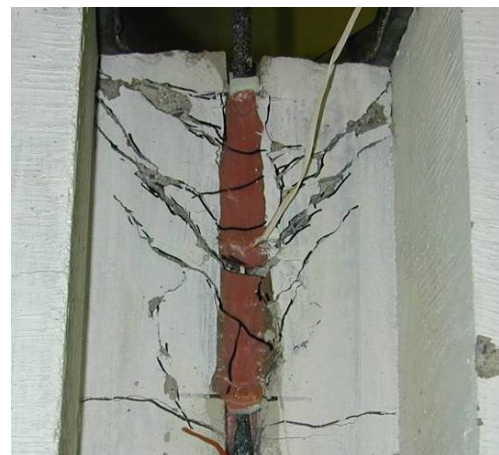


b) Bar slip for N/G-13-E-2.0-12

Fig. 6 - Mode of failure for specimens with NSM-GFRP bar and epoxy adhesive.

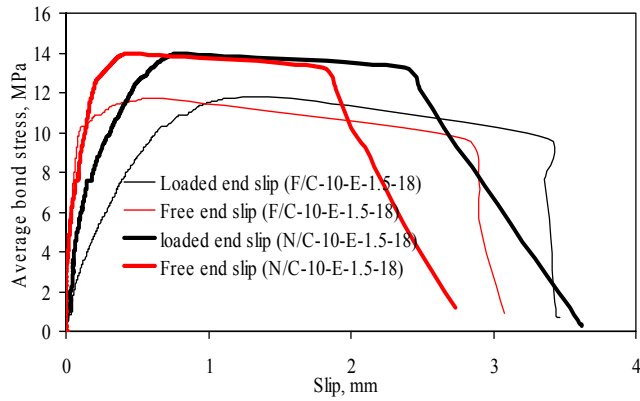


a) Splitting of epoxy covers (F/C-10-E-1.5-12)



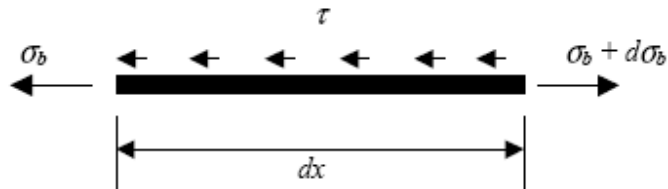
b) Concrete tension failure with longitudinal and transverse cracks in epoxy (F/C-10-E-1.5-18)

Fig. 7 - Modes of failure for the conditioned NSM-CFRP specimens with epoxy adhesive



1

2 Fig. 8 - Average bond stress-slip for specimens N/C-10-E-1.5-18 and F/E-10-1.5-18

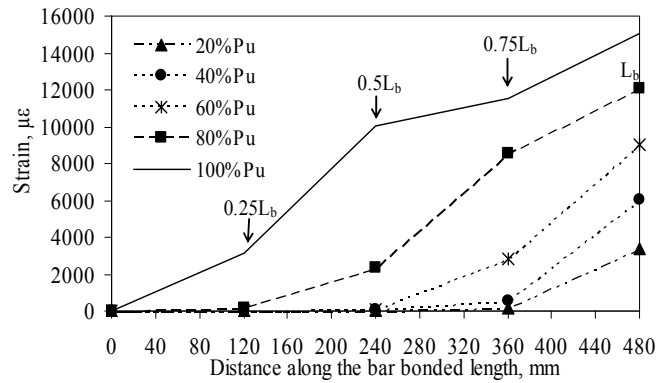


3

4

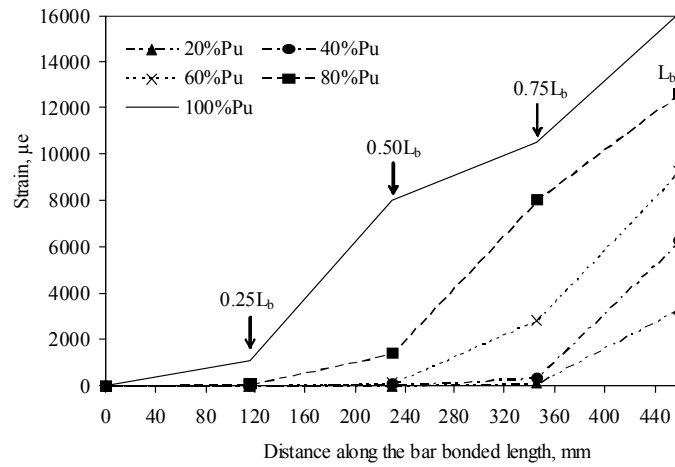
Fig. 9 - Equilibrium forces for NSM bar

5



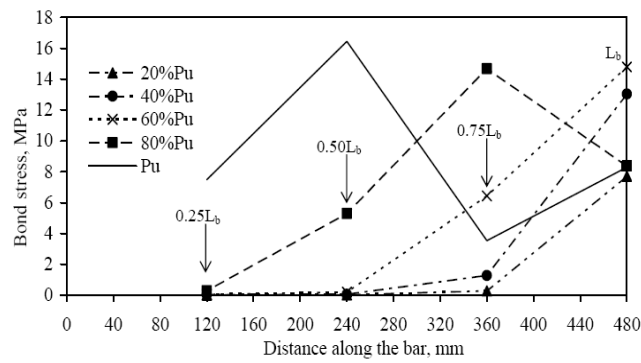
6

7 Fig. 10 - Strain distribution along the bar bonded length for specimen N/C-10-E-1.5-48



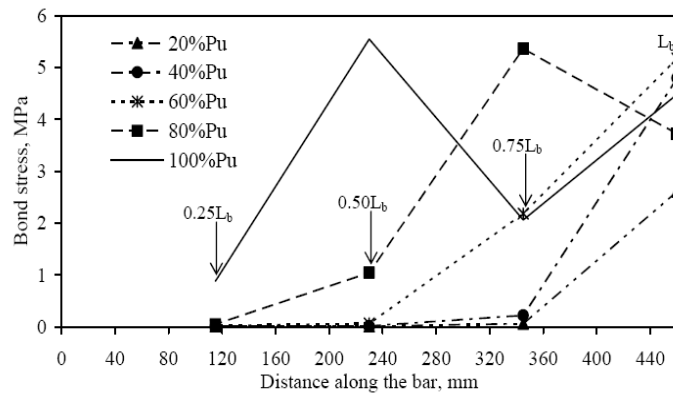
1

2 Fig. 11 - Strain distribution along the bar bonded length for specimen N/G-13-E-2.0-36



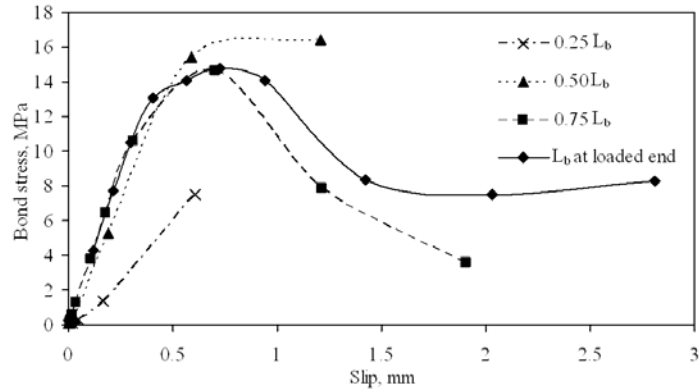
3

4 Fig. 12 - Bond stress distributions along the bar bonded length for specimen N/C-10-E-1.5-48



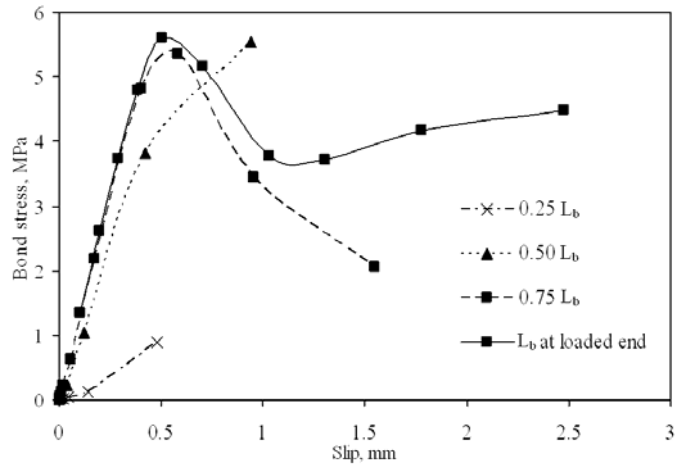
5

6 Fig. 13 - Bond stress distributions along the bar bonded length for specimen N/G-13-E-2.0-36



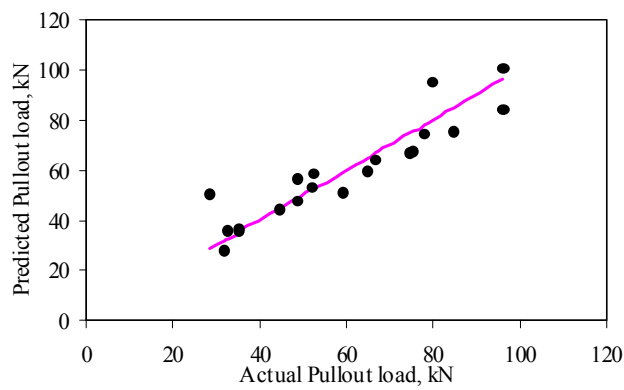
1
2
3

Fig. 14 - Local bond stress-slip at different locations along the bar bonded length for specimen N/C-10-E-1.5-48



4
5
6

Fig. 15 - Local bond stress-slip at different locations along the bar bonded length for specimen N/G-13-E-2.0-36



7
8
9

Fig. 16 - Comparisons between load predictions from the regression models and the experimental results